MDPI

Article

Effect of Ca/Mg on Distribution and Morphology of MnS Inclusions in 45MnVS Non-Quenched and Tempered Steel

Lijuan Su [1], Jun Tian [1,*], Shaoyan Hu [1,*], Ming Lv [2], Xianglong Li [1], Tianpeng Qu [1], Deyong Wang [1] and Tianyin Zhan [1]

1   School of Iron and Steel, Soochow University, Suzhou 215021, China
2   Laiwu Branch, Shan Dong Iron and Steel Corp Ltd., Laiwu 271105, China
*   Correspondence: jtian@suda.edu.cn (J.T.); syhu616@suda.edu.cn (S.H.)

Abstract: The influence of Ca treatment, Mg treatment and Ca–Mg combined treatment on the inclusions in 45MnVS non-quenched and tempered steel were studied in the present work. After the melting experiment, a hot rolling test was carried out on the steel ingot. Additionally, the composition, quantity and morphology of inclusions in the test steel samples were analyzed by automatic scanning electron microscopy (ASPEX) and an energy dispersive X-ray spectrometer connected to scanning electron microscope (SEM-EDS). The results indicated that the inclusions in 45MnVS steel mainly consisted of a large amount of sulfides and a small amount of oxides. Sulfide inclusions could be nucleated and precipitated using oxides as a core during solidification. The proportion of spindle-shaped inclusions in sulfide with smaller sizes was higher. The sizes of MnS–oxide inclusions were larger than those of MnS. After hot rolling, the proportion of spindle-shaped MnS and complex sulfides with oxide cores in the samples was increased significantly. Compared with Ca treatment and Ca–Mg treatment, more oxides were formed in the steel with Mg treatment, which can in turn become the cores for sulfide nucleation and precipitation. Thus, the proportion of MnS–oxide inclusions in steel increased. Compared with Ca treatment and Mg treatment, steel with Ca–Mg treatment was more conducive to the formation of complex sulfides, and increased the proportion of spindle-shaped sulfides in 45MnVS steel. After Ca treatment, Mg treatment and Ca–Mg combined treatment, the proportions of spindle-shaped sulfides in steel were 23.31%, 19.39% and 43.24%, respectively.

Keywords: non-quenched and tempered steel; calcium treatment; magnesium treatment; inclusions; sulfides

1. Introduction

Non-quenched and tempered steel is a typical, medium carbon, special steel with 0.3~0.6 wt% C, and has been rapidly developed in recent years [1]. Additionally, non-quenched and tempered steel has the characteristic of a simplified production process, which can omit the quenching-tempering, straightening and relieving stress operations. It has the advantage of excellent mechanical properties; therefore, the steel has been widely used in automobile engine connecting rods, front axle, steering knuckle and other parts [2–4].

With the continuous modernization in industry, the requirements for material performance are getting higher and higher [5,6]. High quality steels require an optimized control of non-metallic inclusions. The shape, size, quantity and distribution of inclusions have a great influence on the microstructure and properties of steel [7–9]. Non-metallic inclusions essentially reflect the cleanliness of steel, which is closely related to many defects in steel products [10–13]. For the purpose of improving the machinability of steel, medium sulfur content is usually added into the steel. For non-quenched and tempered steel, MnS that is large and more globular provides a benefit to the machinability and retards the grain growth of the steel [14–16]. Therefore, MnS is a typical inclusion detected in non-quenched and tempered steel.

The morphology of MnS inclusions has a great influence on the mechanical properties of steel. Maciejewski [17] studied the effects of sulfide inclusions on mechanical properties and failures of steel components, finding that the ductile manganese sulfides affect the fatigue endurance limit, fatigue crack propagation rate, fracture toughness, notch toughness and transverse tensile properties. Large-sized MnS can be deformed along the longitudinal direction during the hot rolling process and the elongated MnS inclusions will lead to the anisotropy of the mechanical properties of steel, which has a significant impact on the transverse impact toughness and fatigue limit properties of non-quenchable and tempered steel [18,19]. Consequently, numerous research works, focusing on the control of the size, distribution and morphology of MnS inclusions in steel, have been undertaken. Manganese sulfide inclusions were categorized into three different types according to their morphologies: (1) randomly dispersed globular sulfides (type I), (2) the rod-like or dendritic fine sulfides (type II), or (3) the angular sulfides (type III) [20]. Type II sulfides are flexible and can be deformed and become long after rolling, which will seriously reduce the transverse impact toughness of the steel and have a detrimental effect on the steel performance. Additionally, most of the MnS in steel are type II sulfides in sulfur steel. Zhang et al. [21,22] analyzed the size of inclusions in steel with different sulfur contents and calculated the precipitation of MnS by thermodynamics. They found that the shape of inclusions changed from a particle shape to a strip shape when the sulfur content was increased, and the inclusion ratio of Al_2O_3 was significantly reduced in the Al_2O_3–CaO–MgO–MnS quaternary inclusion system with increased MnS content. Previous studies have showed that MnS inclusions with small aspect ratios have little effect on the properties of steel [23].

Various measures have been taken to control the morphology of sulfides during the smelting process for reducing its harmful effects and improving the comprehensive mechanical properties of non-quenched and tempered steel. Sulfide has a strong tendency to precipitate around the oxide inclusions to form complex inclusions, and the deformation of complex sulfide inclusions will be controlled. Calcium treatment is usually used to modify the MnS inclusions. Miao et al. [24] analyzed the coarsening mechanisms of MnS inclusions in Ca-treated steels, and they found that the inclusions in Ca-enriched steel were CA_x, Al_2O_3, CaS, CaS–other and CaS–MnS, and the precipitated S in the form of CaS suppressed the formation of MnS inclusions. Zhang et al. [25] have studied the inclusion evolution after Ca treatment; their results showed that the typical inclusions generated in steel are irregular Al_2O_3–CaO–CaS-type complex inclusions. Compared with Ca, Mg has stronger affinity to sulfur, and inclusions in the steel treated with Mg have been better modified [26]. The results of research by Zhang et al. [27] showed that magnesium treatment could effectively change the morphology of sulfides, and a large number of MnS were transformed into MgO·MgS or MgO–MgS–MnS complex inclusions in high S-content experimental steel. The number and diameter of inclusions in all experimental steel samples were controlled well, helping to improve the properties of the steel. In conclusion, the morphology and size of inclusions in steel can be efficiently controlled by Mg and Ca composite treatment. Shi et al. [28] investigated the formation and disappearance mechanisms of intermediate CaS during Mg–Ca treatment, revealed by thermodynamic calculations. They found that when Mg and Ca were added to molten steel, the typical inclusions were Al–Mg–Ca–O–S complex inclusions, while CaS was an intermediate product. Additionally, they evaluated the effects of various alloying elements on the microstructure of MnS. Combined thermodynamic calculations with high temperature experiments showed that the morphology, size and uniformity of MnS inclusions can be optimized. In conclusion, the morphology and size of inclusions in steel can be efficiently controlled by Mg and Ca composite treatment.

Therefore, in this paper, calcium alloy and/or magnesium alloy was added into 45MnVS non-quenched and tempered steel to research the influence of different alloys on the composition, size, morphology and distribution of inclusions in steel, which can provide a reference for the control of inclusions in non-quenched and tempered steel, and sulfides in sulfur-containing steel.

2. Experimental and Analysis Methodology

The tests were carried out in a 50 kg vacuum induction melting furnace with 45MnVS free cutting non-quenched and tempered steel. The materials were first melted in the furnace, and then calcium and/or magnesium alloy was added into the molten steel. Here, calcium wire was used in Ca treatment, Mg 20% in Ni alloy was used in Mg treatment and calcium wire and Mg 20% in Ni alloy were used in Ca–Mg combined treatment. Lastly, ferrous sulfides were added into the molten steel. After the composition of liquid steel was homogenized, the molten steel was cast in a cast iron mold. The compositions of the steel ingot are listed in Table 1. The steel sample with Ca treatment is denoted as S1, and the other two samples with Mg treatment and Ca–Mg treatment are denoted as S2 and S3, respectively. The content of S in the three steel samples is similar; the values are 0.046 wt%, 0.050 wt% and 0.047 wt%, respectively. Additionally, the O contents are 0.0021 wt%, 0.0028 wt% and 0.0019 wt%, respectively.

Table 1. Chemical compositions of the steels used in experiments (mass%).

Steel	C	Si	Mn	P	S	Al	V	Ca	Mg	O
S1	0.44	0.49	1.38	0.006	0.046	0.021	0.11	0.0009	-	0.0021
S2	0.45	0.58	1.47	0.007	0.050	0.016	0.12	-	0.0011	0.0028
S3	0.45	0.51	1.43	0.005	0.047	0.024	0.10	0.0007	0.0009	0.0019

The steel ingot was hot rolled into a sheet material with a thickness of about 13 mm. The shape of the rolled products on the paper is shown in Figure 1. Metallographic samples with a size of $15 \times 13 \times 10$ mm^3 were taken from the three sheets. A schematic diagram of the sampling location in the rolled metal is shown in Figure 2. The samples were ground and polished to prepare them for the inclusion inspection. The chemical compositions of the inclusions were analyzed by an energy dispersive X-ray spectrometer (EDS) connected to scanning electron microscope (SEM). In addition, automatic scanning electron microscopy (ASPEX) was applied for statistical analysis of the number of inclusions in a longitudinal section of the rolled metal. The minimum width of detectable inclusions was set at 0.5 μm.

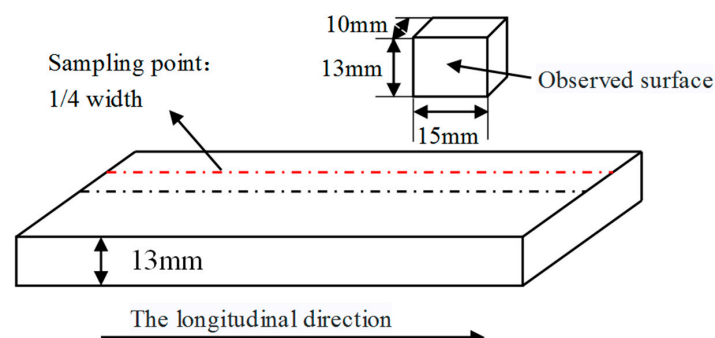**Figure 1.** The shape of the rolled products.

Figure 2. Schematic diagram of sampling in rolled metal.

3. Results

3.1. Types of Inclusions in Rolled Samples

ASPEX was used for statistical analysis of the inclusions in the three samples, and the results are shown in Table 2. It can be seen that the quantitative density of inclusions in samples S2 and S3 is higher than that in sample S1; the values are 225, 306 and 390 per mm^2, respectively. According to the classification of inclusions listed in Table 3, inclusions detected in the experimental samples can be classified into three types as MnS, MnS–oxide and the other type.

Table 2. The quantitative density of inclusions in samples.

Steel	Scanning Area, mm^2	Inclusion Quantity	Quantitative Density of Inclusions, /mm^2
S1	20.75	4666	225
S2	24.90	7617	306
S3	29.88	11,650	390

Table 3. Classification principle of inclusions.

Types of Inclusions	Classification Principle (the Detected Element Content of Inclusions)	Remarks
MnS	Al = 0, Mn > 0, S > 0	MnS without an oxide core
MnS–oxide	Al > 0, Mn > 0, S > 0	MnS with an oxide core
Other type	Failing to meet the requirements conditions above	Inclusions except MnS or MnS–oxide

The quantity percentage of the three types of inclusions in the experimental samples was calculated based on the classification principle above. The results are represented in Figure 3. As shown in Figure 3, most inclusions in the steels were MnS and MnS–oxide complex inclusions. The quantity percentages of sulfide inclusions were 92.31%, 94.91% and 85.87%, respectively. Figure 4 shows quantity percentage of the types of sulfide inclusions. As can be seen, there are a large number of MnS–oxide complex inclusions which were formed with an oxide core in samples S2 and S3. The proportion of MnS–oxide complex inclusions in the steels increased rapidly after Mg treatment and Ca–Mg treatment.
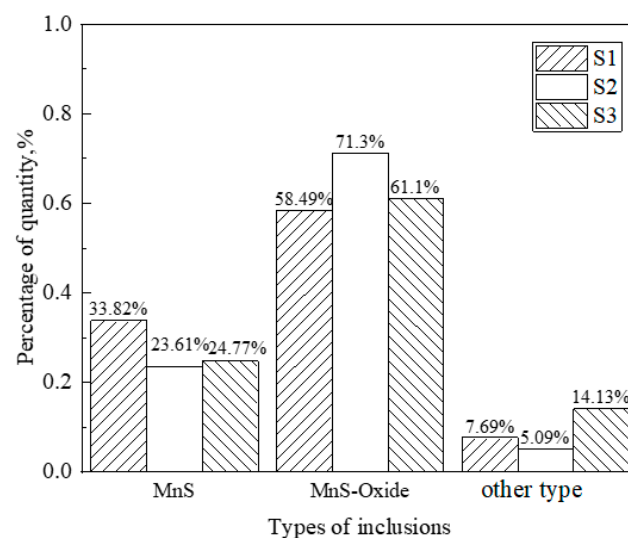

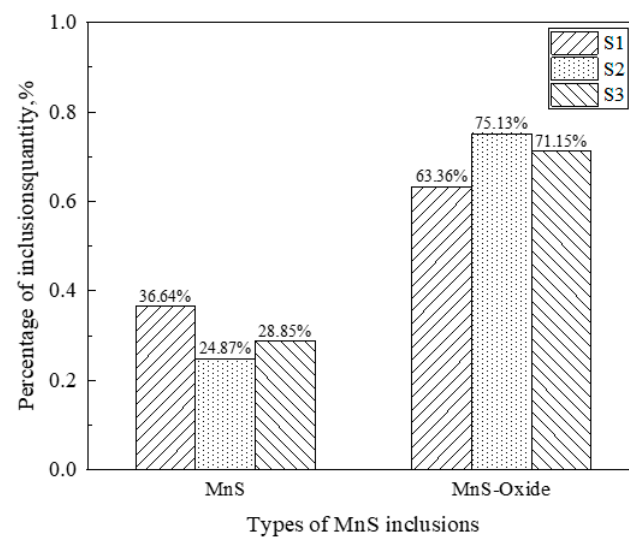**Figure 3.** Types and percentage of inclusions in samples.

Figure 4. Types and percentage of sulfides in samples.

3.2. Morphology and Size of MnS Inclusions in Rolled Samples

The morphology of inclusions affect the mechanical properties of steel. Diederichs [29] found that large-sized elongated MnS inclusions lead to the anisotropic properties of steel. Therefore, in this paper, the aspect ratio of sulfide in the rolled samples was analyzed statistically. Sulfides with an aspect ratio of 3 or less were defined as spindle-shaped sulfides. The aspect ratio of all sulfides in the samples was statistical analyzed by ASPEX. The proportion of spindle-shaped MnS is shown in Figure 5. The proportion of spindle-shaped MnS–oxide was significantly higher than that of spindle-shaped MnS. The proportion of spindle-shaped MnS–oxide in sample S3 with Ca–Mg treatment was as high as 51.92%, while the proportion of spindle-shaped MnS in sample S2 with Mg treatment was just 10.07%. The proportions of spindle-shaped sulfides in samples S1, S2 and S3 were calculated, and the values are 23.31%, 19.39% and 43.24%, respectively.
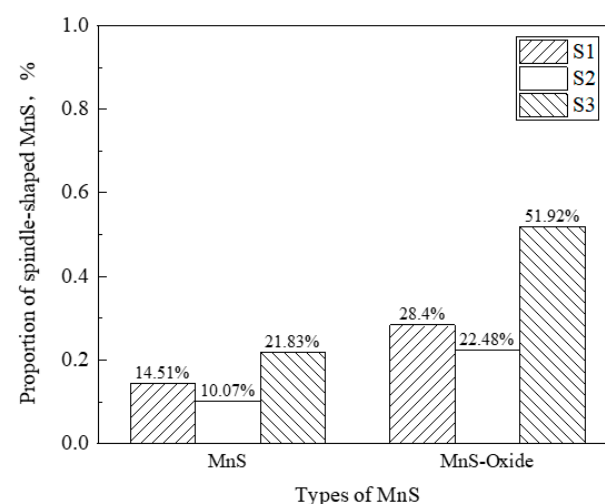

Figure 5. Percentage of spindle-shaped MnS in different types of sulfides.

Figure 6 shows the morphologies of sulfide inclusions in the rolled steel samples. The MnS inclusions in the steels were mostly elongated. It was found that almost all sulfide inclusions in the steel without an oxide core were typical elongated MnS. The lengths of the elongated MnS inclusions were about 20 μm; however, occasionally the lengths were larger than 30 μm. The spindle-shaped MnS–oxide inclusions precipitated with oxide as the core. Usually, the sizes of spindle-shaped MnS–oxide were in the range of 1 μm

to 5 μm. Elemental analyses for typical MnS–oxide complex inclusions were carried out by SEM-EDS, and are shown in Figure 6. It was clear that S was distributed around the oxide inclusions such as Al_2O_3 or $MgO \cdot Al_2O_3$. Compared with inner oxides, sulfides were presented as a light grey. Lu et al. [30] investigated the effect of oxides on the characteristics of MnS in a Al-killed non-quenched and tempered steel, finding that in low Ca bearing steel, $MgO \cdot Al_2O_3$ (MA) and MnS are main inclusions and MA oxides have a high ability to perform MnS heterogeneous nucleation.
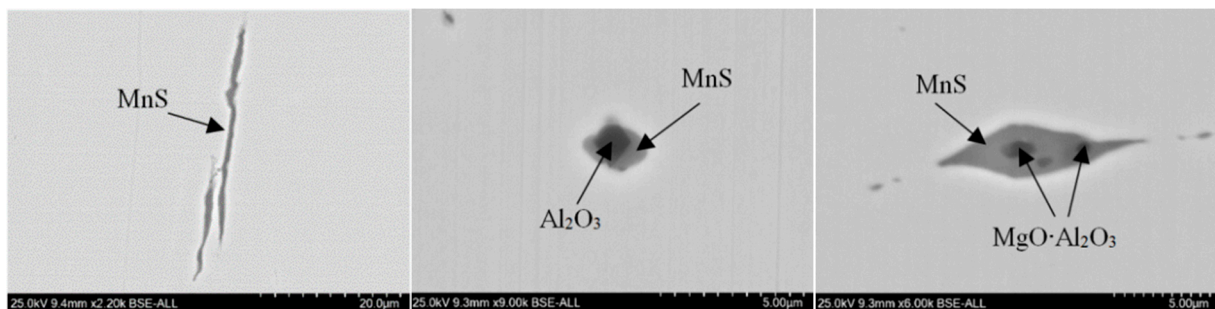
Figure 6. SEM morphologies of elongated and spindle-shaped MnS in rolled steel samples.

Inclusions in steels will deform along the rolling direction during the hot rolling process. Therefore, the morphology of inclusions will change in the rolled material. Thus, the length or width of deformed inclusions cannot describe the sizes of inclusions efficiently. Therefore, the areas of inclusion were used to represent its sizes in this work. The areas of all inclusions in samples S1, S2 and S3 were statistically analyzed by ASPEX. The proportion of area distribution of the three types of inclusions in the rolled steel samples is shown in Figure 7. The percentages of MnS–oxide and MnS inclusions were 44.67% and 66.16%, respectively, in the area range of 0 μm^2 to 10 μm^2 in sample S1. The percentages of MnS–oxide and MnS inclusions were 38.26% and 73.41%, respectively, in the area range of 0 μm^2 to 10 μm^2 in sample S2. The percentages of MnS–oxide and MnS inclusions were 61.44% and 95.39%, respectively, in the area range of 0 μm^2 to 10 μm^2 in sample S3. The percentages of MnS–oxide inclusions with an area greater than 20 μm^2 were 39.87%, 34.8% and 25.37% in sample S1, S2 and S3, respectively, which were higher than that of MnS in the same sample. This means that MnS–oxide inclusions had larger areas than pure MnS inclusions in the rolled steel samples. Hence, we can indicate that MnS–oxide has a larger average size than MnS. Compared with Ca treatment (S1) and Mg treatment (S2), steel with Ca–Mg treatment (S3) was more conducive to the formation of small-sized complex MnS–oxide inclusions.
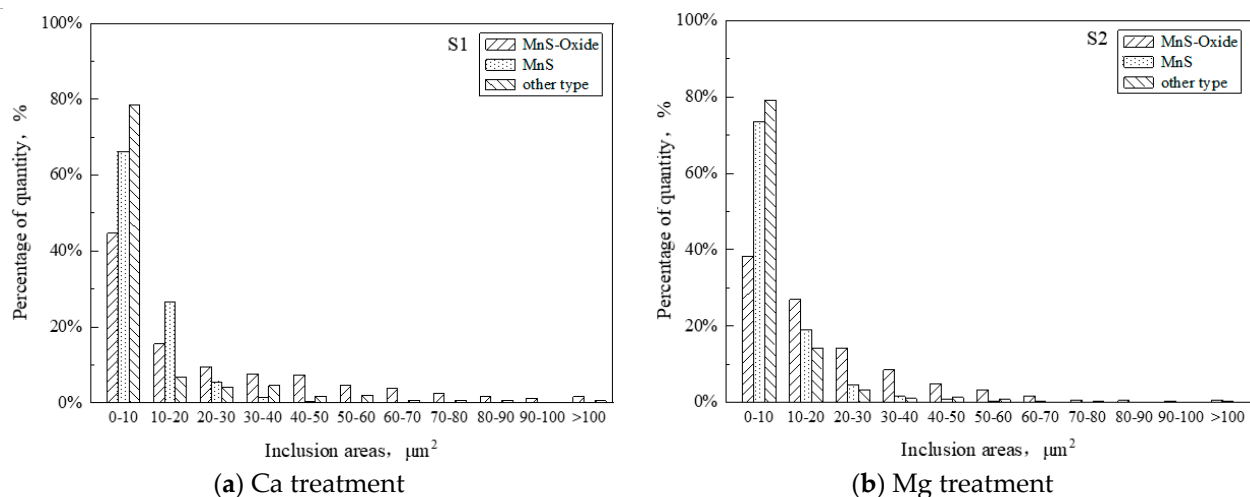

(a) Ca treatment
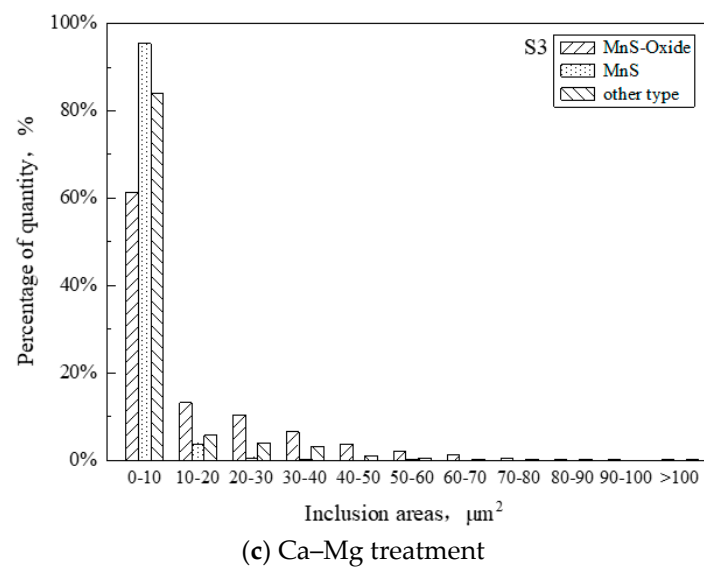

(b) Mg treatment

Figure 7. *Cont.*

(c) Ca–Mg treatment

Figure 7. Area distribution of inclusions in rolled steel samples.

4. Discussion

4.1. The Formation of Inclusions in Steel

The formation of inclusions in the 45MnVS non-quenched and tempered steel during the solidification process after adding S was calculated using Factsage 8.0 software (thermfact/CRCT and GTT-Technologies, Montreal, Canada and Aachen, Germany). The initial S content in the experimental steel was about 0.003 wt%. The equilibrated components of the molten steel and slag at 1600 °C were calculated by the Equilib module in Factsage software. Then, according to the chemical compositions of steels in Table 1, the inclusion contents during the solidification process of the steels S1, S2 and S3 were calculated. The results are shown in Figures 8–10. Liquidus and solidus temperatures of 45MnVS steels with the chemical compositions listed in Table 1 were calculated by Equations (1) and (2) [22]. The calculated values of liquidus and solidus temperatures are marked in Figures 8–10.

$$T_{\text{liq}} = 1536 - 83w[\text{C}] - 7.8w[\text{Si}] - 5w[\text{Mn}] - 32w[\text{P}] - 31.5w[\text{S}] - 3.6w[\text{Al}] - 2w[\text{V}] \quad (1)$$

$$T_{\text{sol}} = 1536 - 334w[\text{C}] - 12.3w[\text{Si}] - 6.8w[\text{Mn}] - 124.5w[\text{P}] - 183.5w[\text{S}] - 4.1w[\text{Al}] \quad (2)$$
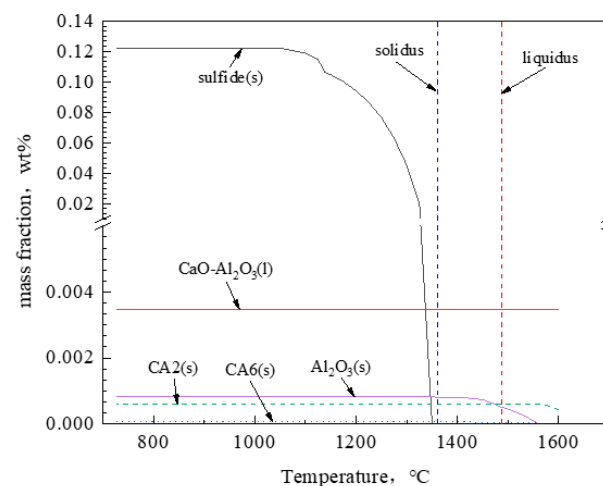

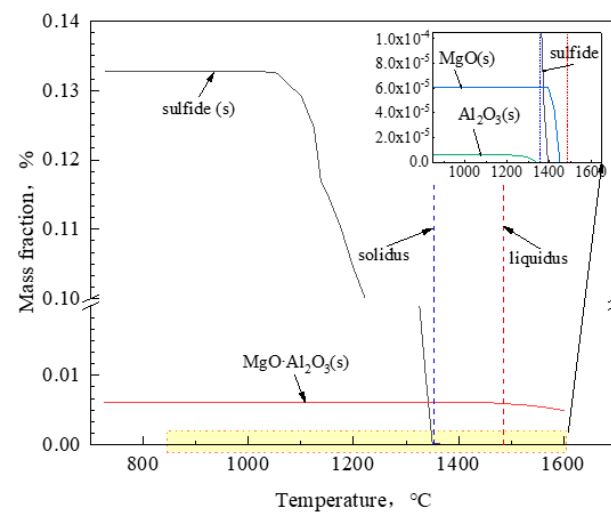**Figure 8.** Inclusion content during solidification of sample S1.

Figure 9. Inclusion content during solidification of sample S2.
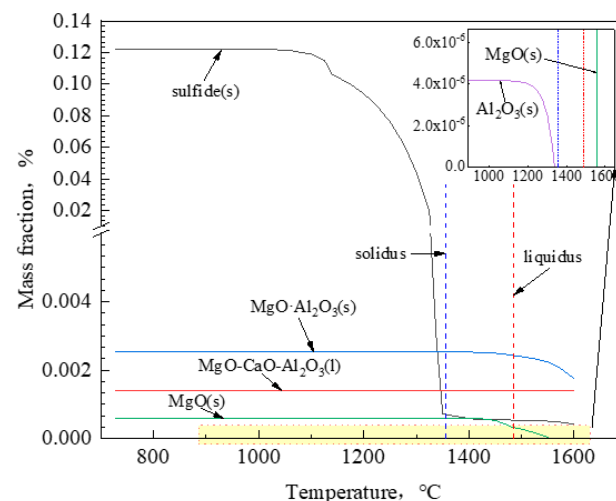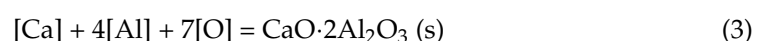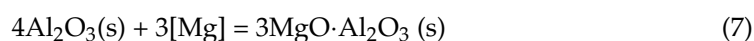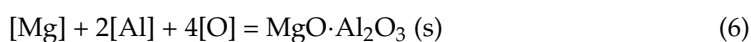

Figure 10. Inclusion content during solidification of sample S3.

As can be seen from Figure 8, liquid $CaO–Al_2O_3$ was generated in sample S1 after addition of the calcium wire. In addition, oxide inclusions in the form of Al_2O_3, CA2 and a small amount of CA6 (where C represents CaO and A represents Al_2O_3) were formed in molten steel as shown in Equations (3)–(5). All oxide inclusions were formed above the liquidus temperature. CA2 was formed at 1600 °C, and its content increased with the decrease in temperature. The content of CA2 reached a maximum and remained unchanged at 1560 °C. At the same time, CA6 begins to form at 1560 °C in molten steel. Additionally, at 1355 °C, the reaction shown in Equation (4) ended, and the content of CA6 reached a maximum and remained unchanged. In molten steel, Al_2O_3 inclusions are formed by reactions among dissolved Al and O, which is shown in Equation (5). The reaction in Equation (5) was carried out at 1550 °C and ended at 1078 °C. The Al_2O_3 inclusion content increased with the decrease in temperature during the reaction process. Additionally, at the end of solidification, the mass fraction of Al_2O_3 was about 5.93×10^{-4} wt%. Sulfide began to form at 1350 °C, which was below the solidus temperature of sample S1. The content of sulfide increased with decreasing temperature and stabilized at 0.122 wt% at 767 °C.

$$[Ca] + 4[Al] + 7[O] = CaO·2Al_2O_3 \text{ (s)} \tag{3}$$

$$[Ca] + 12[Al] + 19[O] = CaO·6Al_2O_3 \text{ (s)} \tag{4}$$

$$2[Al] + 3[O] = Al_2O_3 \text{ (s)} \tag{5}$$

As can be seen from Figure 9, the oxide inclusions in sample S2 were mainly $MgO \cdot Al_2O_3$ spinel and a small amount of MgO and Al_2O_3. In molten steel, $MgO \cdot Al_2O_3$ can be formed by direct reactions among dissolved Mg, Al and O, which is shown in Equation (6). Since Mg has a strong affinity with O in molten steel, Mg will also react with Al_2O_3 to form $MgO \cdot Al_2O_3$ spinel, as shown in Equation (7), after addition of Mg–Ni alloy. $MgO \cdot Al_2O_3$ spinel inclusions were formed at 1600 °C as shown in Equations (6) and (7). The content of $MgO \cdot Al_2O_3$ increased with the decrease in temperature, and stabilized at 0.0061 wt% at 1375 °C. Then, a small amount of sulfides were formed by the reaction among dissolved Mn and S in molten steel. The sulfide content increased with the decrease in temperature and increased rapidly below 1325 °C, reaching a maximum of 0.1327 wt% at 843 °C. In sample S2, the reaction in Equation (5) was carried out at 1325 °C, which was under the solidus temperature. At the end of the reaction, the content of Al_2O_3 was just 1×10^{-5} wt% at 1078 °C.

$$[Mg] + 2[Al] + 4[O] = MgO \cdot Al_2O_3 \text{ (s)} \tag{6}$$

$$4Al_2O_3(s) + 3[Mg] = 3MgO \cdot Al_2O_3 \text{ (s)} \tag{7}$$

$$[Mg] + [O] = MgO \text{ (s)} \tag{8}$$

As can be seen from Figure 10, liquid $MgO–CaO–Al_2O_3$ was generated in sample S3 after Ca–Mg treatment. The oxide inclusions in sample S3 were $MgO \cdot Al_2O_3$ spinel, MgO and a small amount of Al_2O_3. In molten steel, $MgO \cdot Al_2O_3$ was formed by the reaction shown in Equations (6) and (7). The content of $MgO \cdot Al_2O_3$ inclusions increased with the decrease in temperature, and stabilized at 0.0025 wt% at 1350 °C. In molten steel S3, MgO inclusions were formed by the reaction shown in Equation (8) among dissolved Mg and O at 1550 °C, which was above the liquidus temperature of sample S3. The reaction ended at 1425 °C and the content of MgO remained at 7.5×10^{-5} wt%. Al_2O_3 inclusions were formed by the reaction shown in Equation (5). The reaction occurred at 1325 °C, which was below the solidus temperature. The content of Al_2O_3 increased with the decrease in temperature. At the end of the reaction, the content of Al_2O_3 was just 4.15×10^{-6} wt% at 1077 °C. Sulfides were formed at 1600 °C. The content of sulfides increased with the decrease in temperature and increased rapidly at 1325 °C, reaching a maximum of 0.12 wt% at 792 °C.

Based on the analysis above, it was obvious that oxide inclusions in non-quenched and tempered steel after Ca treatment were mainly Al_2O_3, while the oxide inclusions were mainly $MgO \cdot Al_2O_3$ after Mg treatment and the combined Ca–Mg treatment in samples S2 and S3. The theoretical calculation results showed that all the Al_2O_3 and $MgO \cdot Al_2O_3$ oxides were formed above the liquidus temperatures of the steels; therefore, the sulfides formed during the solidification process can be nucleated and precipitated with the oxides, as shown in Figure 6. As can be seen from Figures 3 and 4, compared to Ca treatment and Ca–Mg treatment, the percentage of oxides in sample S2 with Mg treatment was the largest. This was mainly due to the formation of a certain amount of liquid oxides such as $CaO–Al_2O_3$ in sample S1 and $MgO–CaO–Al_2O_3$ in sample S3 after Ca treatment and Ca–Mg treatment. Abdelaziz et al. [31] has studied the effect of Ca on the cleanliness of low carbon aluminum killed steel. Their studies showed that calcium aluminate can be formed by adding a small amount of Ca, while the amount of CaS was very small. In research by Yang et al. [32], they showed that magnesium treatment products can finely disperse the inclusions in molten steel. Similar work has also been pursued by others [26], in which MnS inclusion modification of re-sulfurized special steel was studied using Mg–Ca alloys in a steel plant. Therefore, more oxides were formed in sample S2 which can provide more nucleation cores for the precipitation of sulfide, and the number of MnS inclusions containing oxide cores in sample S2 was relatively high. Zhang et al. [27] put forward a proposed model for the formation mechanism of complex oxysulfide inclusions. In this model, oxide particles form primarily at an appropriate addition amount of alloy in molten steel. Secondly, the dissolved S and Mn diffuse toward the surface of oxide particles. Then,

a product layer of MnS forms quickly. As time goes on, more and more MnS generates and forms a thicker layer covering the surface of the oxide cores. As the MnS–oxide complex inclusions nucleate and precipitate with oxide cores, the precipitation temperature of these inclusions increases compared to MnS. At the same time, the precipitation temperature range of MnS–oxide inclusions increases, which means that this type of inclusion had a longer time to grow than that of MnS. Therefore, the areas of inclusions of MnS–oxide were relatively larger than that of MnS, as shown in Figure 7.

4.2. Change in Morphology of MnS–Oxide Inclusions

The mechanical properties are influenced by the type, shape and size of sulfides. It is necessary to control the morphology and size of sulfides in the medium- and high-sulfur content steels in order to optimize the mechanical properties of the steel. Therefore, in practical production, fine spindle-shaped complex sulfides are obtained as much as possible. The aspect ratio is one of the most important parameters to describe the inclusion morphology [33]. There are a large number of MnS inclusions in 45MnVS non-quenched and tempered steel which are easily deformed during the rolling process. Research has shown that improper control of MnS inclusions will seriously affect the mechanical properties of steel [17]. According to Diederichs' categorization [20], type II sulfides have a bad effect on the steel performance, so it is necessary to increase the resistance of MnS to deformation to reduce the harmful effect on products. Type I and type III sulfides are more resistant to deformation and are less harmful, which is desired in non-quenched and tempered steel. Many measures have been taken to change the morphology of sulfide inclusions to make them spindle-shaped. If the aspect ratio of inclusions is less than 3, the resistance of the inclusions to deformation increases.

In the present study, it was found that the sulfide inclusions in the samples show a difference in morphology and distribution after the addition of Ca and/or Mg alloys. Based on the analysis above, it can be seen from Figure 3 that sulfides were mostly included in the test steel, which were mainly MnS and MnS–oxide. The proportion of spindle-shaped inclusions in MnS–oxide was higher than that of MnS in samples S1, S2 and S3. Additionally, the proportion of spindle-shaped inclusions was the highest in Ca–Mg-treated sample S3. The relationship between the content of Ca and Mg in MnS and the shape of MnS is shown in Figure 11. MnS inclusions containing a certain amount of Ca and Mg are more likely to be spindle-shaped. Research by Jiang et al. [34] showed that there was an effective effect on controlling the morphology of sulfides with Ca and Mg. After addition of Ca and Mg, MnS, CaS and MgS–(Mn, Me)S complex sulfides (where, Me represents Ca and Mg) were formed. The MnS, CaS and MgS sulfides had good deformation resistance at high temperature, so the aspect ratio of complex sulfides was reduced in the rolling process. Figure 11 shows that more Ca and Mg were dissolved in MnS inclusions in sample S3 with Ca–Mg treatment. Therefore, the proportion of spindle-shaped MnS in sample S3 was the largest, as shown in Figure 5.

The sulfide inclusions form in molten steel as shown in Equations (9)–(11) after Ca or Mg treatment [35,36].

$$[Mg] + [S] = MgS \text{ (s)} \tag{9}$$

$$[Ca] + [S] = CaS \text{ (s)} \tag{10}$$

$$[Mn] + [S] = MnS \text{ (s)} \tag{11}$$
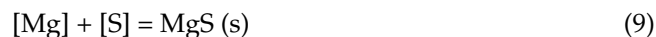
MnS inclusions will precipitate with oxides as the core during the process of steel solidification, as shown in Figure 6. The MnS precipitates around Mg oxide (MgO or $MgO \cdot Al_2O_3$; under the test conditions in this paper, it is mainly $MgO \cdot Al_2O_3$ spinel inclusion) or the S in molten steel will react with the MgO in the inclusions, as shown in Equations (12) and (13). At this time, the complex sulfides (Mn,Mg)S–oxide are formed. Similarly, the complex sulfides (Mn,Ca)S–oxide are formed as the MnS precipitates around Ca oxide (C_mA_n), or the S in molten steel will react with the CaO in the inclusions, as shown in Equations (14) and (15).
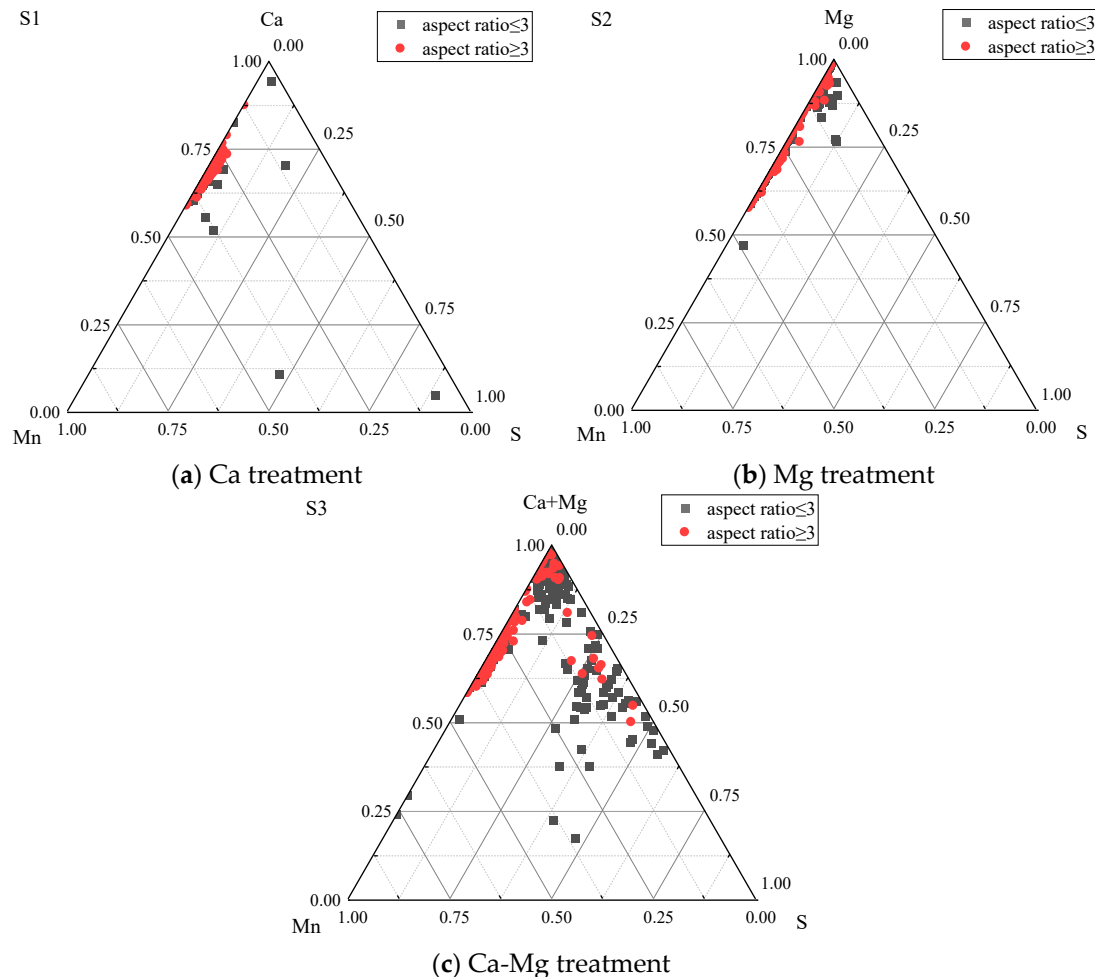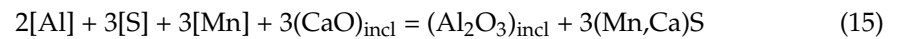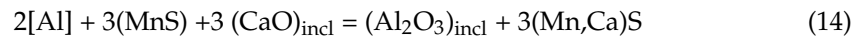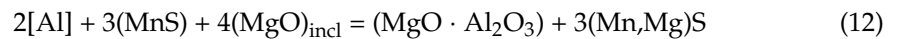
$$2[Al] + 3(MnS) + 4(MgO)_{incl} = (MgO \cdot Al_2O_3) + 3(Mn,Mg)S \qquad (12)$$

$$2[Al] + 3[S] + 3[Mn] + 4(MgO)_{incl} = (MgO \cdot Al_2O_3) + 3(Mn,Mg)S \qquad (13)$$

$$2[Al] + 3(MnS) + 3(CaO)_{incl} = (Al_2O_3)_{incl} + 3(Mn,Ca)S \qquad (14)$$

$$2[Al] + 3[S] + 3[Mn] + 3(CaO)_{incl} = (Al_2O_3)_{incl} + 3(Mn,Ca)S \qquad (15)$$

(**a**) Ca treatment

(**b**) Mg treatment

(**c**) Ca-Mg treatment

Figure 11. Relationship between content of Ca and Mg and aspect ratio in MnS.

The formation of complex sulfides in samples S1, S2 and S3 was calculated by Factsage8.0 software simulation as shown in Figure 12. The temperature ranges for formation of the complex sulfides in samples S1, S2 and S3 were 20 °C, 45 °C and 230 °C, respectively. Compared with the Ca treatment and Mg treatment in samples S1 and S2, the temperature range for complex sulfide formation was larger in samples S3 with Ca–Mg treatment. Meanwhile, the mass fractions of sulfides were 12.23%, 13.32% and 12.49% in the experimental steels because they can provide more nucleation cores for precipitation of sulfide with Mg treatment, which was consistent with the results in Figure 8 to Figure 10.

Since the Ca content in sample S1 and Mg content in sample S2 were lower than the total content of Ca and Mg in sample S3, in order to reduce the influence of Ca and Mg content differences on the temperature range of complex sulfides formation, the Ca content in sample S1 was increased to 20×10^{-4} wt%, and the Mg content in sample S2 was increased to 20×10^{-4} wt%, equaling the contents of Ca and Mg in sample S3, while the contents of other elements remained unchanged. The temperature range for complex sulfides formation was calculated by Factsage 8.0 using the same method, and the results

are shown in Figure 13. Compared with Figures 12 and 13, the temperature ranges for complex sulfide formation were 47 °C and 58 °C when the contents of Ca and Mg were both 20×10^{-6}, which is far less than 230 °C with the same contents for Ca–Mg–treated steel in sample S3. Therefore, under the conditions of the same added alloy content, the Ca–Mg composite-treated non-quenched and tempered steel had the largest temperature range for complex sulfide formation. This is beneficial to the formation of complex sulfides, and increased the proportion of spindle-shaped sulfide in steels.
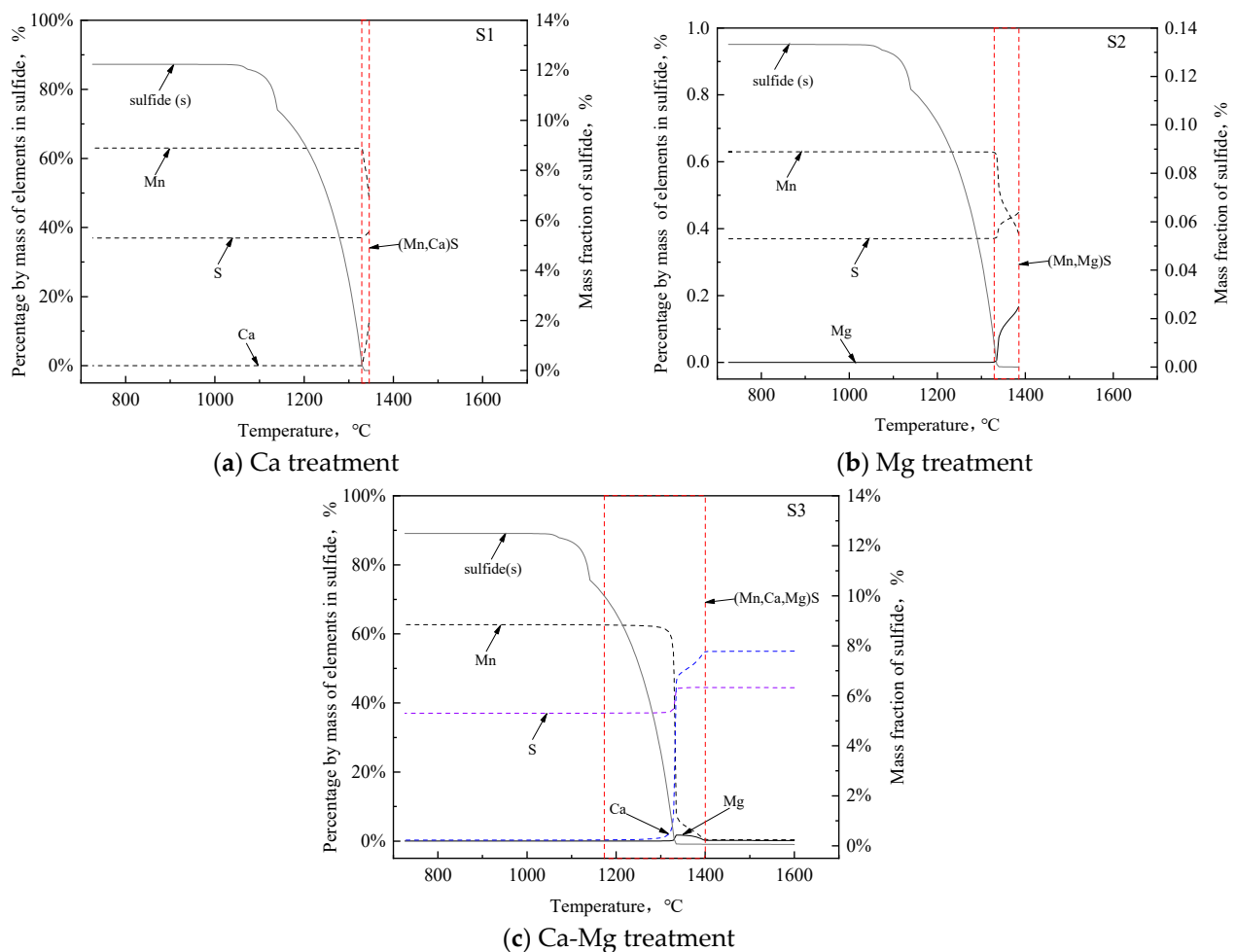
Figure 12. Temperature range for formation of complex sulfides.

According to the statistical method in Figure 7, the proportion of spindle-shaped sulfides in MnS and MnS–oxide inclusion types of different area sizes was statistical analyzed, and the results are shown in Figures 14 and 15. As can be seen from Figure 14, the percentages of spindle-shaped sulfides in MnS with the areas of 0 mm^2 to 10 mm^2 were 17.62%, 9.55% and 22.19% for samples S1, S2 and S3, respectively, which decreased to 8.85%, 6.41% and 8.18%, respectively, with areas of 10 mm^2 to 20 mm^2 in the experimental samples. Figure 15 shows that the percentages of spindle-shaped sulfides in MnS–oxides were higher with the areas of 0 mm^2 to 40 mm^2, and the percentages reduced when the inclusion area was greater than 40 mm^2. Therefore, the proportion of spindle-shaped sulfides in sulfides was lower with a larger area in the MnS and MnS–oxide sulfide types. The data in Figures 14 and 15 were line-fitted for further discussions and conclusions. It can be seen that the proportion of spindle-shaped MnS and MnS–oxide sulfides decreased with the increase in the size. Segal [37] studied the influence of MnS size on the deformation characteristics of manganese sulfide inclusions in steel, and the results showed that the deformation degree of MnS with a smaller size was lower than that of MnS with a larger

size under the same deformation conditions. In this paper, the experimental allowed for us to reach the same conclusion.
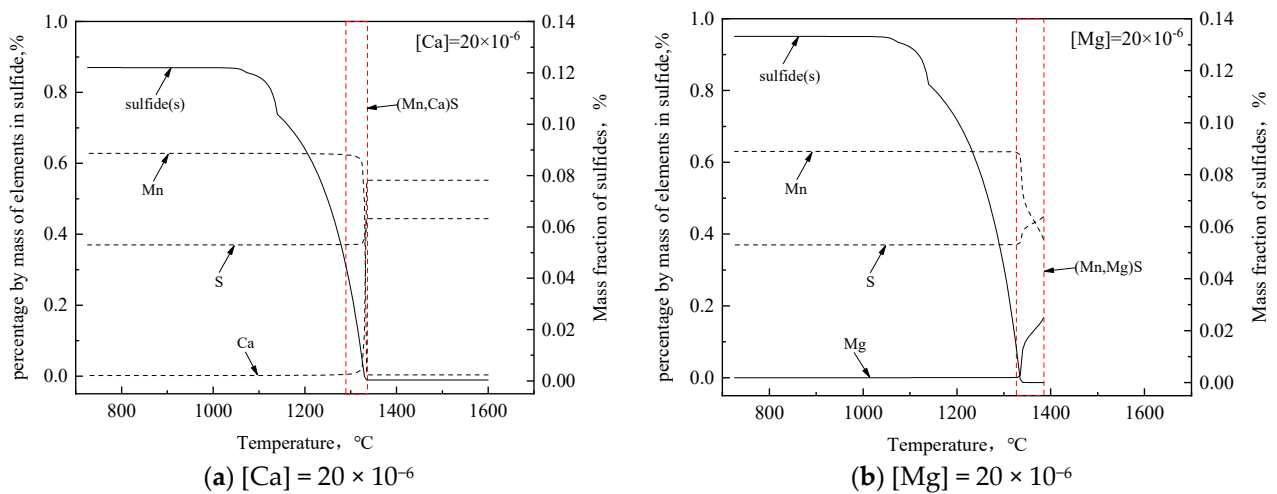

(**a**) [Ca] = 20 × 10⁻⁶ (**b**) [Mg] = 20 × 10⁻⁶

Figure 13. Temperature range for complex sulfide formation when the contents of Ca and Mg are both 20×10^{-6}.
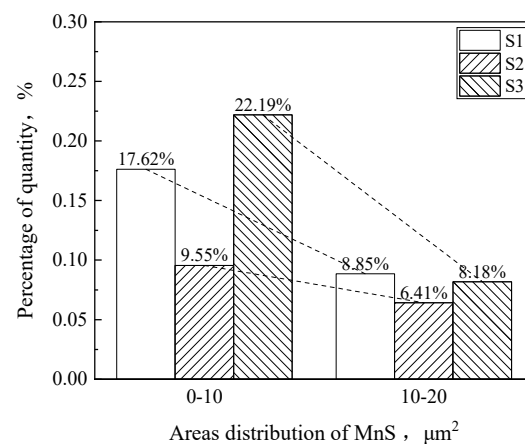

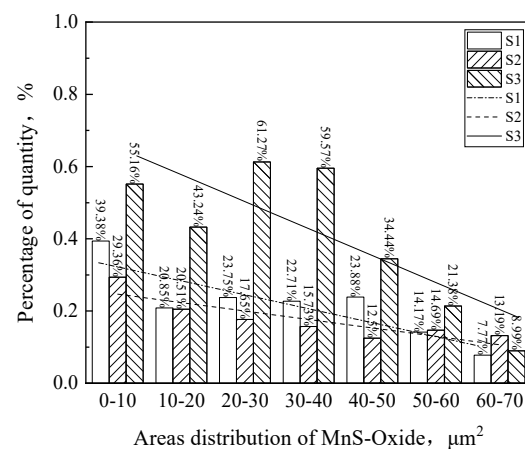**Figure 14.** Proportion of spindle–shaped sulfides in MnS with different area sizes.

Figure 15. Proportion of spindle–shaped sulfides in MnS–oxide with different area sizes.

Through the above analysis, the measures to improve the proportion of spindle-shaped sulfides in steel can be concluded as follows: (1) increase the proportion of com-

pound sulfides in steels, (2) increase the proportion of sulfides containing oxide cores, and (3) reduce the sizes of sulfides in steels.

5. Conclusions

In this paper, Ca and Mg alloys were added into 45MnVS non-quenched and tempered steels in a vacuum induction furnace. The hot rolling test was carried out on the steel ingots, and the composition and morphology of inclusions in the rolled steel samples were analyzed. The following conclusions are obtained:

(1) The inclusions in 45MnVS non-quenched and tempered steel were mainly sulfides and a small amount of oxides. Oxide inclusions were mainly formed above the liquidus temperature and sulfides were formed during solidification. Sulfides could be nucleated and precipitated using oxides as a core during solidification.

(2) The proportion of spindle-shaped inclusions in sulfides increases by reducing the sizes of inclusions. The sizes of MnS–oxide inclusions was larger than those of MnS inclusions. The spindle-shaped inclusions were easily formed in MnS, CaS and MgS–(Mn, Me)S complex sulfides and MnS–oxide which contained an oxide core.

(3) Compared with Ca treatment and Ca–Mg treatment, more oxide inclusions were formed in steel with Mg treatment, which can become a core for sulfide nucleation and precipitation. Thus, the proportion of MnS–oxide inclusions in steel increased in sample S2.

(4) Compared with Ca treatment and Mg treatment, steel with a combined CaMg treatment was more conducive to the formation of complex sulfides and increased the proportion of spindle-shaped sulfides in sample S3.

(5) After Ca treatment, Mg treatment and Ca–Mg combined treatment, the proportion of spindle-shaped sulfides in the samples was 23.31%, 19.39% and 43.24%, respectively.

References

1. Luo, Y.Z.; Zhang, J.M.; Liu, Z.M.; Wu, S.Z. In situ observation and thermodynamic calculation of MnS in 49MnVS3 non-quenched and tempered steel. *Acta Metall. Sin.* **2011**, *24*, 326–334. [CrossRef]
2. Chen, Y.; Ma, M.; Wang, G. Resent progress of non-quenched and tempered steel for automotive sheet. *Eng. Sci.* **2014**, *2*, 41–45.
3. Zhou, B.; Shen, Y.; Tan, L.; Yang, H.X.; Cao, W.Q.; Bao, Y.Z. Research on a new process of the non-quenched and tempered steel with high strength and high toughness. *Phys. Procedia* **2013**, *50*, 25–31. [CrossRef]
4. Lu, J.L.; Cheng, G.G.; Che, J.L.; Wang, L.S.; Xiong, G.J. Effect of oxides on characteristics of MnS and transverse mechanical properties in commercial Al-Killed non-quenched and tempered steel. *Met. Mater. Int.* **2019**, *25*, 473–486. [CrossRef]
5. Kuz'min, M.P.; Kuz'mina, Y.M.; Kuz'min, P.B. Production of primary silumins ingots modified with strontium. *Solid State Phenom.* **2021**, *316*, 490–495. [CrossRef]

6. Kuz'min, M.P.; Kuz'mina, Y.M.; Kuz'mina, A.S. Production and properties of aluminum-based composites modified with carbon nanotubes. *Mater. Today Proc.* **2019**, *19*, 1826–1830. [CrossRef]
7. Ei Koussy, M.R.; Ei Mahallawi, I.S.; Khalifa, W.; Dawood, M.M.; Bueckins, M. Effects of thermal aging on microstructure and mechanical properties of duplex stainless steel weldments. *Mater. Sci. Technol.* **2004**, *20*, 375–381. [CrossRef]
8. Park, J.H.; Zhang, L.F. Kinetic modeling of nonmetallic inclusions behavior in molten steel: A Review. *Metall. Mater. Trans. B* **2020**, *51*, 2453–2482. [CrossRef]
9. Zhang, Y.X.; Chen, C.; Lin, W.M.; Yu, Y.C.; E, D.Y.; Wang, S.B. Numerical Simulation of Tracers Transport Process in Water Model of a Vacuum Refining Unit: Single Snorkel Refining Furnace. *Steel Res. Int.* **2020**, *91*, 2000022. [CrossRef]
10. Anmark, N.; Karasev, A.; Jonsson, P.G. The Effect of Different Non-Metallic Inclusions on the Machinability of Steels. *Materials* **2015**, *8*, 751–783. [CrossRef]
11. Podder, A.; Coley, K.S.; Phillion, A.B. Modeling Study of Steel-Slag-Inclusion Reactions During the Refining of Si-Mn Killed Steel. *Steel Res. Int.* **2022**, *93*, 2100831. [CrossRef]
12. Fan, J.; Li, Y.; Chen, C.; Ouyang, X.; Wang, T.; Lin, W. Effect of Uniform and Non-Uniform Increasing Casting Flow Rate on Dispersion and Outflow Percentage of Tracers in Four Strand Tundishes under Strand Blockage Conditions. *Metals* **2022**, *12*, 1016. [CrossRef]
13. Chen, C.; Ni, P.Y.; Jonsson, L.T.I.; Tilliander, A.; Cheng, G.G.; Jönsson, P.G. A Model Study of Inclusions Deposition, Macroscopic Transport, and Dynamic Removal at Steel–Slag Interface for Different Tundish Designs. *Metall. Mater. Trans. B* **2016**, *47*, 1916–1932. [CrossRef]
14. Yang, H.X.; Ren, Y.; Ji, S.; Zhang, L.F. Modification of Sulfides in a High Sulfur Steel by Cerium Addition. *Metall. Mater. Trans. B* **2022**, *53*, 3992–4005. [CrossRef]
15. Tinoco, H.A.; Fintove, S.; Heikkila, I.; Heereo, D.; Vuoristo, T.; Dlouhy, I. Experimental and numerical study of micromechanical damage induced by MnS-based inclusions. *Mater. Sci. Eng. A* **2022**, *856*, 144009. [CrossRef]
16. Kang, J.; Yu, Y.C.; Zhang, J.L.; Chen, C.; Wang, S.B. Effect of Rare Earth on Inclusion Evolution in Industrial Production of HRB500E Steel. *Metall. Res. Technol.* **2021**, *118*, 220. [CrossRef]
17. Maciejewski, J. The Effects of Sulfide Inclusions on Mechanical Properties and Failures of Steel Components. *J. Fail. Anal. Prev.* **2015**, *15*, 169–178. [CrossRef]
18. Lv, Z.A.; Ni, H.; Zhang, H.; Liu, C.S. Evolution of MnS inclusions in Ti-bearing X80 pipeline steel. *J. Iron Steel Res. Int.* **2017**, *24*, 654–660. [CrossRef]
19. Xie, J.B.; Hu, D.L.; Fu, J.X.; Liu, H. Numerical analysis of effect of the solutes on formation of MnS in non-tempered steel. *Ironmak. Steelmak.* **2019**, *46*, 542–549. [CrossRef]
20. Diederichs, R.; Bleck, W. Modelling of manganese sulphide formation during solidification, part I: Description of MnS formation parameters. *Steel Res. Int.* **2006**, *77*, 202–209. [CrossRef]
21. Zhang, H.L.; Feng, G.H.; Liu, X.; Wang, B.S.; Liu, X.M. Effect of Sulfur Content on the Composition of Inclusions and MnS Precipitation Behavior in Bearing Steel. *Metals* **2020**, *10*, 570. [CrossRef]
22. Tian, J.; Qu, T.; Wang, D.; Wang, H.; Xu, Z.; E, X.R. Effect of Mg and Ca on the Characteristics of Inclusions in Sulphur Steel. *Arch. Metall. Mater.* **2018**, *63*, 1599–1607. [CrossRef]
23. Chu, J.H.; Zhang, L.Q.; Yang, J.; Bao, Y.P.; Ali, N.; Zhang, C.J. Characterization of precipitation, evolution, and growth of MnS inclusions in medium/high manganese steel during solidification process. *Mater. Charact.* **2022**, *194*, 112367. [CrossRef]
24. Miao, K.Y.; Nabeel, M.; Dogan, N. Coarsening Mechanisms of CaS Inclusions in Ca-Treated Steels. *Metals* **2022**, *12*, 707. [CrossRef]
25. Zhang, T.; Liu, C.; Mu, H.; Li, Y.; Jiang, M. Inclusion evolution after calcium addition in Al-killed steel with different sulphur content. *Ironmak. Steelmak.* **2018**, *45*, 447–456. [CrossRef]
26. Shen, P.; Fu, J. Morphology study on inclusion modifications using Mg-Ca treatment in resulfurized special steel. *Materials* **2019**, *12*, 197. [CrossRef]
27. Zhang, T.; Wang, D.; Liu, C.; Jiang, M.; Lu, M.; Wang, B.; Zhang, S. Modification of inclusions in liquid iron by Mg treatment. *J. Iron Steel Res. Int.* **2014**, *21*, 99–103. [CrossRef]
28. Shi, L.; Zhou, X.; Wang, D.; Qu, T.; Wang, H.; Zhu, J. Evolution of Inclusions in Magnesium-Calcium-Treated Liquid Iron. *Metals* **2021**, *11*, 1213. [CrossRef]
29. Diederichs, R.; Bulte, R.; Pariser, G.; Bleck, W. Modelling of manganese sulphide formation during solidification, part II: Correlation of solidification and MnS formation. *Steel Res. Int.* **2006**, *77*, 256–264. [CrossRef]
30. Lu, J.; Cheng, G.; Chen, L.; Xiong, G.; Wang, L. Distribution and morphology of MnS inclusions in resulfurized non-quenched and tempered steel with Zr addition. *ISIJ Int.* **2018**, *58*, 1307–1315. [CrossRef]
31. Abdelaziz, S.; Megahed, G.; Ei Mahallawi, I.; Ahamed, H. Control of Ca addition for improved cleanness of low C, Al killed steel. *Ironmak. Steelmak.* **2009**, *36*, 432–441. [CrossRef]
32. Yang, J.; Yamasaki, T.; Kuwabara, M. Behavior of inclusions in deoxidation process of molten steel with in situ produced Mg vapor. *ISIJ Int.* **2007**, *47*, 699–708. [CrossRef]
33. Ghosh, A.; Modak, P.; Chakrabarti, D. Effect of MnS inclusion and crystallographic texture on anisotropy in Charpy impact toughness of low carbon ferritic steel. *Mater. Sci. Eng. A* **2016**, *654*, 298–308. [CrossRef]
34. Jiang, L.; Cui, K. Experimental study and thermodynamical calculation on the formation of eutectic phase of MnS-RE2S3 and (Mn,Ca)S-RE2S3 in sulfur-containing free-cutting steel. *J. Rare Earths* **1992**, *10*, 114–120.
35. Suito, H.; Inoue, R. Thermodynamics on control of inclusions composition in ultra-clean steels. *ISIJ Int.* **1996**, *36*, 528–536. [CrossRef]

36. Fu, J.; Yu, Y.G.; Wang, A.R.; Chen, B.P.; Sun, W.S. Inclusion modification with Mg treatment for 35CrNi3MoV steel. *J. Mater. Sci. Technol.* **1998**, *14*, 53–56.

37. Segal, A.; Charles, J. Influence of particle size on deformation characteristics of manganese sulphide inclusions in steel. *Met. Technol.* **1977**, *4*, 177. [CrossRef]